

Correlation between baryonic process and galaxy assembly bias

ZILAN XIAO,^{1,2} JUNYU HUA,^{1,2} ZHONGXU ZHAI,^{1,2,3,4} ANDREW BENSON,⁵ AND YUN WANG⁶

¹*State Key Laboratory of Dark Matter Physics, Tsung-Dao Lee Institute & School of Physics and Astronomy, Shanghai Jiao Tong University, Shanghai 200240, China*

²*Shanghai Key Laboratory for Particle Physics and Cosmology, and Key Laboratory for Particle Physics, Astrophysics and Cosmology, Ministry of Education, Shanghai Jiao Tong University, Shanghai 200240, China*

³*Waterloo Center for Astrophysics, University of Waterloo, Waterloo, ON N2L 3G1, Canada*

⁴*Department of Physics and Astronomy, University of Waterloo, Waterloo, ON N2L 3G1, Canada*

⁵*Carnegie Observatories, 813 Santa Barbara Street, Pasadena, CA 91101, USA*

⁶*IPAC, California Institute of Technology, Mail Code 314-6, 1200 E. California Blvd., Pasadena, CA 91125, USA*

(Received Month DD, YYYY; Revised Month DD, YYYY; Accepted Month DD, YYYY)

Submitted to ApJ

ABSTRACT

Galaxy assembly bias (GAB) is the dependence of galaxy clustering on secondary properties beyond halo mass. In this work, we study the connections between GAB and baryonic processes using the GalactiCus semi-analytic model (SAM) for galaxy formation and evolution applied to the UNIT simulation. By generating hundreds of galaxy mocks with varying parameters governing gas cooling, star formation, stellar feedback, and AGN feedback, we employ a shuffling method to quantify the GAB signal and compare the contributions of halo concentration and local environment to GAB. Using the Random Forest algorithm, we evaluate the importance of different baryonic processes for GAB. We find that for stellar-mass-selected galaxies, the dominant baryonic processes are gas cooling and stellar feedback, and the result does not change significantly with the number density; for SFR-selected galaxies, the primary process shifts from star formation to gas cooling as the number density increases. These results establish a direct and quantitative link between baryonic physics and GAB, which can provide guidance for empirical GAB parameterizations in upcoming and future galaxy surveys.

Keywords: cosmology: galaxies: formation — galaxies: haloes — galaxies: statistics — cosmology: theory — dark matter — large-scale structure of Universe

1. INTRODUCTION

In the current paradigm of galaxy formation, galaxies form and evolve within dark matter halos, and their properties are intimately connected to their host halos. Modeling the connection between galaxies and halos not only helps to understand the physical processes of galaxy formation, but also helps to constrain cosmological parameters through galaxy surveys, such as SDSS-I/II (D. G. York et al. 2000; K. N. Abazajian et al. 2009), 2dFGRS (M. Colless et al. 2001; S. Cole et al. 2005), WiggleZ (M. J. Drinkwater et al. 2010), BOSS (K. S. Dawson et al. 2012), eBOSS (K. S. Dawson

et al. 2016) and DESI (D. Collaboration et al. 2016; A. Adame et al. 2025). In recent years, advances in large-scale galaxy surveys and high-resolution numerical simulations have led to the emergence of numerous models to describe the statistical galaxy–halo connection (R. H. Wechsler & J. L. Tinker 2018). In general, these models can be divided into two categories: empirical models, such as subhalo abundance matching (SHAM) (A. V. Kravtsov et al. 2004; A. Tasitsiomi et al. 2004; A. Vale & J. P. Ostriker 2004) and the halo occupation distribution (HOD) (Y. P. Jing et al. 1998; A. J. Benson et al. 2000; J. A. Peacock & R. E. Smith 2000; U. Seljak 2000; M. White et al. 2001; A. A. Berlind & D. H. Weinberg 2002; A. Cooray & R. Sheth 2002; Z. Zheng et al. 2005); and physical models, such as hydrodynamic simulations (M. Vogelsberger et al. 2014; A. Pillepich et al. 2017; R. Pakmor et al. 2023) and semi-analytical models (SAM)

(S. D. M. White & C. S. Frenk 1991; S. Cole et al. 2000; A. J. Benson 2010; Q. Guo et al. 2012). Due to the high-resolution and large-scale computing requirements, hydrodynamic simulations consume substantial computing resources, thereby limiting both the simulation volume and the ability to thoroughly explore the parameter space, although they can model galaxies in great detail. On the other hand, SAMs can approximate many astrophysical processes of galaxy formation and evolution with empirical prescriptions, thereby accelerating computations and overcoming the above limitations of fully exploring the parameter space.

In the excursion set formalism and the basic structure formation scenario, the clustering of dark matter halos is influenced solely by their mass (W. H. Press & P. Schechter 1974; J. R. Bond et al. 1991). However, it is observed in N-body simulations that halo clustering can also depend on other halo properties beyond mass, including formation time, concentration, and spin (L. Gao et al. 2005; R. H. Wechsler et al. 2006; L. Gao & S. D. M. White 2007; Y. Li et al. 2008). This phenomenon is now generally termed halo assembly bias (HAB). These additional properties are collectively referred to as secondary halo properties, and the dependency of clustering on them is referred to as secondary bias (Y.-Y. Mao et al. 2017). Throughout this paper, we refer to this effect as assembly bias for simplicity.

In empirical models, such as the standard HOD, the occupation of galaxies in halos depends only on halo mass. However, the assembly history of halos not only affects the clustering of halos but also may affect the occupation of galaxies in halos, showing occupation variation (OV) (X. Xu et al. 2021a). It denotes the differences in the occupation of galaxies residing in halos of the same mass. For example, older halos tend to have a higher probability of hosting a central galaxy at low masses; however, among halos of the same mass, older halos contain fewer satellite galaxies than younger ones (S. Contreras et al. 2019). This OV combined with HAB indicates that the clustering properties of galaxies are determined by host halo mass and secondary halo properties, i.e. galaxy assembly bias (GAB).

This phenomenon was noticed by D. J. Croton et al. (2007) using a SAM applied to the Millennium Simulation. S. Contreras et al. (2019) studied how the influence of the halo concentration and halo age on HAB, OV, and GAB evolves with redshift. The results show that the halo age-based GAB mainly comes from OV, while the concentration-based GAB mainly comes from HAB. X. Xu et al. (2021a) further analyzed the contributions of various secondary properties to GAB, including internal properties such as halo age, concentration, and angular

momentum, as well as various external environmental factors. The results seem to show that the local environment is the most important secondary property for GAB (B. Hadzhiyska et al. 2020; X. Xu et al. 2021a; S. Yuan et al. 2021b).

On the other hand, observational evidence for GAB remains inconclusive. Some studies have reported positive detections (M. C. Cooper et al. 2010; L. Wang et al. 2013; H. Miyatake et al. 2016; A. R. Zentner et al. 2019; A. Obuljen et al. 2020; S. Yuan et al. 2021a,b), while others have found the impact of assembly bias to be small or consistent with zero (M. R. Blanton & A. A. Berlind 2007; Y.-T. Lin et al. 2016; Y. Zu & R. Mandelbaum 2016; K. Walsh & J. Tinker 2019; A. N. Salcedo et al. 2022; Z. Shao et al. 2025). While the observational status of GAB remains debated, a number of studies have focused on parameterizing GAB in theoretical models to enable controllable mock catalogues and facilitate future detection. Previous studies have successfully incorporated GAB into empirical models, including composite abundance matching (B. V. Lehmann et al. 2016; S. Contreras et al. 2021) and modified HOD models (A. P. Hearin et al. 2016b; J. E. McEwen & D. H. Weinberg 2018; B. D. Wibking et al. 2018; H.-G. Yang et al. 2026). These theoretical models of GAB rely on secondary halo properties as phenomenological proxies, while the connection between baryonic processes and the GAB remains largely unexplored. M. P. van Daalen et al. (2014) found that AGN feedback removes material from the inner regions of subhaloes, lowering their central density concentration and making them less compact at fixed mass. Such internal structural changes affect the spatial distribution and clustering of subhaloes on small to intermediate scales. H.-G. Yang et al. (2026) compared the redshift evolution of GAB in two hydrodynamical simulations, SIMBA and IllustrisTNG. They found that the divergent GAB trends at $z < 2$ can be attributed to differences in AGN feedback implementation, suggesting that baryonic physics plays a crucial role in shaping GAB. This indicates that the impact of baryonic effects on GAB deserves further investigation.

As mentioned earlier, hydrodynamic simulations can be ideal to study the baryonic effect. However, it is not feasible to sample the parameter space with sufficient volume and obtain a robust clustering measurement. Therefore, we turn to SAMs and examine the impacts of various baryonic effects on the GAB signatures in this work. In SAM, galaxy formation and evolution are driven by processes including gas cooling, star formation, supernova feedback, active galactic nucleus (AGN) feedback, etc (A. J. Benson 2010; R. H. Wechsler & J. L. Tinker 2018). Using the Galacticus SAM and a machine

learning algorithm, we quantify the importance of individual baryonic processes for the GAB signal in galaxy samples selected with different secondary properties and number densities.

This paper is organized as follows. In Section 2, we introduce our data from the UNIT simulation and Galacticus SAM, as well as the secondary halo properties we used to isolate the effect of assembly bias. Section 3 presents our results of OV and GAB, showing their dependence on different secondary properties and galaxy number density, and the dependence of GAB on baryonic processes. Finally, we conclude with a summary and discussion in Section 4.

2. SIMULATION AND METHOD

2.1. UNIT simulation

We build the SAM models using the UNIT cosmological simulation (C.-H. Chuang et al. 2019). This simulation adopts a Planck 2015 cosmology (Planck Collaboration et al. 2016) and evolves 4096^3 dark matter particles within a periodic cubic volume of side length $1 h^{-1}\text{Gpc}$. Dark matter halos are identified using the ROCKSTAR halo finder (P. S. Behroozi et al. 2012a), and merger trees are constructed with the Consistent Tree software (P. S. Behroozi et al. 2012b). With high mass resolution, large volume, and complete merger trees, these outputs enable mock catalogue construction using SAM and subsequent analysis of GAB.

2.2. Galacticus SAM

We employ the Galacticus SAM (A. J. Benson 2012) to build our galaxy catalogues. Following Z. Zhai et al. (2025), we focus on the galaxy sample at $z = 0.55$, which is selected to match the BOSS CMASS compilation. We note that the methodology applied in this work can be extended to other redshifts and galaxy selections. For simplicity, we use the products from our earlier work Z. Zhai et al. (2025) and refer the reader to that work for more details on the SAM modeling; here we only provide a brief summary. In the Galacticus modeling of galaxy formation including star formation, gas cooling, AGN feedback, etc., we allow 16 parameters of these components to vary (see Table 2 in Z. Zhai et al. 2025) and investigate their influence on the GAB signal. The parameter ranges span physically plausible values while allowing significant variation in the resulting galaxy properties. By sampling this multi-dimensional parameter space, we can systematically explore the influence of different baryonic processes on the galaxy-halo connection and the resulting GAB signal.

2.3. Secondary halo properties

In the study of secondary bias of dark matter halos and galaxies, it is crucial to specify the relevant secondary halo properties. These include halo properties beyond mass, such as formation time, concentration, spin, and local environment, which can impact the clustering of both galaxies and dark matter halos. In this study, we focus on two such properties: halo concentration and the local environment to represent internal and external properties, respectively. We note that this choice is not exclusive; a study that fully explores a broader set of properties could provide a more comprehensive evaluation of assembly bias, as in X. Xu et al. (2021a).

(1) Halo concentration c is defined as the ratio between the virial radius r_{vir} and the characteristic scale radius r_s of the Navarro–Frenk–White (NFW) density profile (J. F. Navarro et al. 1996) of a dark matter halo: $c = r_{\text{vir}}/r_s$. The virial radius r_{vir} marks the boundary within which the halo is approximately virialized. The scale radius r_s marks the radial scale where the logarithmic slope of the NFW profile changes. A higher concentration indicates that the halo mass is more centrally concentrated.

(2) The smoothed environmental matter density δ_R is measured using a top-hat window function of radius R . We consider two smoothing scales, $R = 10 h^{-1}\text{Mpc}$ and $R = 5 h^{-1}\text{Mpc}$, denoted as δ_{10} and δ_5 , respectively. These quantities provide a simple but effective measure of the halo’s local environment (J. E. McEwen & D. H. Weinberg 2018).

2.4. Method

We quantify the clustering signals of the galaxies using the two-point correlation function $\xi(r)$, which measures the excess probability of finding a galaxy pair with separation r compared with a random distribution. In order to avoid the complexities of redshift space distortion due to peculiar velocity, all the computation in our work is done in real space.

With the clustering measurements, a straightforward way of evaluating the GAB signal is to split the galaxy sample by halo properties of interest and compare the resultant clustering signal. Alternatively, we employ the shuffling method as widely used in literature (e.g., D. J. Croton et al. 2007; Y. Zu et al. 2008; J. Chaves-Montero et al. 2016; S. Contreras et al. 2019; X. Xu et al. 2021a), i.e. compare the correlation function of the original galaxy sample with that of a shuffled sample. In particular, we shuffle the galaxies among halos within narrow bins of halo mass. The central galaxies are moved to the center of the new halos, and satellite galaxies are moved

together with their central galaxies to keep their positions relative to the centrals. This procedure is able to retain the one-halo clustering term while removing correlations due to halo properties other than mass. The GAB signal is then defined as the difference in the two-point correlation functions before and after this shuffling procedure. For this process, halo mass M_h is binned in $\log_{10} M_h [h^{-1} M_\odot]$. The primary mass range of 9.8–15.2 is divided into equal-width bins of 0.2 dex in our analysis.

We also employ a *double shuffle* method to isolate individual contributions of different secondary properties to the GAB signal (X. Xu et al. 2021a). In this case, we shuffle the galaxies within the same host halo mass and an additional secondary property (concentration, or the local environment δ_{10}, δ_5). The resulting GAB signal thus quantifies the specific influence of that particular secondary property.

3. RESULTS

In this section, we present our main results. We first examine the halo occupation distribution (HOD) of the galaxy mock from our SAM. We then present our evaluation of GAB measurements. Finally, we adopt a random forest method to quantify the impact of various baryonic processes on the significance of GAB signals.

3.1. Occupation variation

Since OV, together with HAB, constitutes the GAB, we first examine the OV to gain insight into the subsequent GAB measurements. To examine the OV with concentration and local environment, we first rank halos within narrow bins of fixed mass according to a given secondary property, and then compare the HOD for the subsets of halos with the highest and lowest 20% of that property.

Fig. 1 illustrates how the halo occupation distribution is influenced by halo concentration and local environment (δ_5, δ_{10}). We generate hundreds of galaxy mocks by varying the physical parameters within the Galacticus SAM framework. The figure presents the results from only a single representative mock for illustration. The red (blue) curves correspond to the 20% of halos with the highest (lowest) concentration or local environmental density. Dashed, dotted and solid curves denote the centrals, satellites and full sample.

The two panels in the rightmost column display the OV for halo concentration. For stellar-mass-selected centrals (top), the HOD of central galaxy rises monotonically from 0 to 1 with halo mass as expected, i.e. the most massive galaxies tend to live in the most massive dark matter halos (M. White et al. 2011). For SFR-

selected centrals (bottom), the HOD exhibits a non-monotonic trend, i.e. star forming galaxies preferentially live in halos of intermediate masses, a phenomena that has been observed in multiple SAM mocks (Z. Zhai et al. 2019; A. Merson et al. 2019).

The impact of concentration differs significantly between stellar-mass-selected and SFR-selected samples for central galaxies. For stellar-mass-selected centrals, high concentration enhances occupation at low masses but suppresses it at high masses, while for SFR-selected centrals, it enhances occupation across the entire mass range.

For satellite galaxies, the dependence on concentration is similar for both stellar-mass-selected and SFR-selected samples. High-concentration halos host fewer satellites than their low-concentration counterparts at fixed halo mass. On average, the impact of concentration is more pronounced for satellites than centrals. These results are largely consistent with S. Contreras et al. (2019).

The four panels in the left and middle columns show the OV attributed to local environment. For stellar-mass-selected samples, halos in denser environments begin to host central galaxies at slightly lower masses and contain slightly more satellites at fixed halo mass. The OV become negligible as the halo mass increases, which is consistent with I. Zehavi et al. (2018) and X. Xu et al. (2021a). Compared to local environment, concentration has a stronger impact on OV. This may be understood in the context of how secondary properties introduce scatter into the stellar mass–halo mass (SMHM) relation. I. Zehavi et al. (2018) found that formation time introduces more scatter to the SMHM relation for central galaxies than does local environment, and such scatter is found to diminish at higher masses. The stronger OV we find for concentration may similarly reflect that concentration introduces greater scatter than environment. However, it is worth noting that the relative strength of OV does not directly or necessarily dictate the contribution to GAB. As will be shown in Sec. 3.2, despite its weaker OV, the local environment contributes a stronger GAB signal than does concentration.

3.2. Galaxy assembly bias

We investigate the GAB signals with different sample selections. The single-shuffled sample, constructed by randomizing galaxy positions among halos of the same mass, serves as a reference devoid of GAB, as it breaks the correlation between galaxy positions and any secondary halo properties beyond mass. The total GAB signal is then quantified by the ratio of the two-point correlation functions from the original and the single-

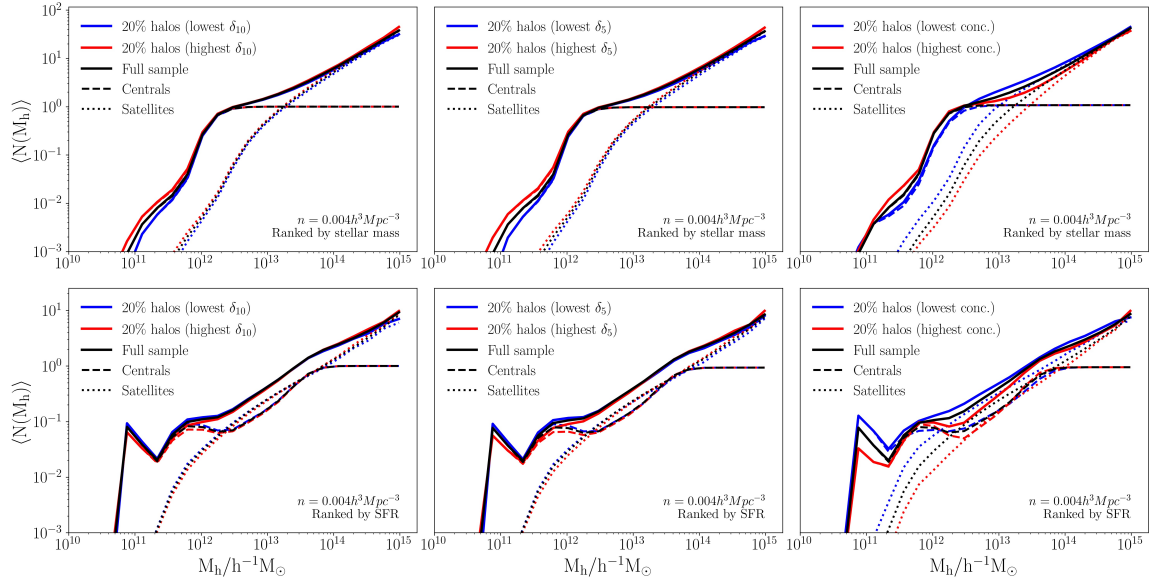


Figure 1. Halo occupation distributions (HODs) for a galaxy mock with number density of $n = 0.004h^3\text{Mpc}^{-3}$. The top and bottom panels correspond to galaxies selected by stellar mass and star formation rate (SFR), respectively. From left to right, the columns show results for δ_{10} , δ_5 , and concentration, respectively. In each panel, red and blue lines correspond to halos with the highest and lowest 20 percent of the given property, while line styles (dashed, dotted, solid) distinguish central, satellites, and the total galaxies.

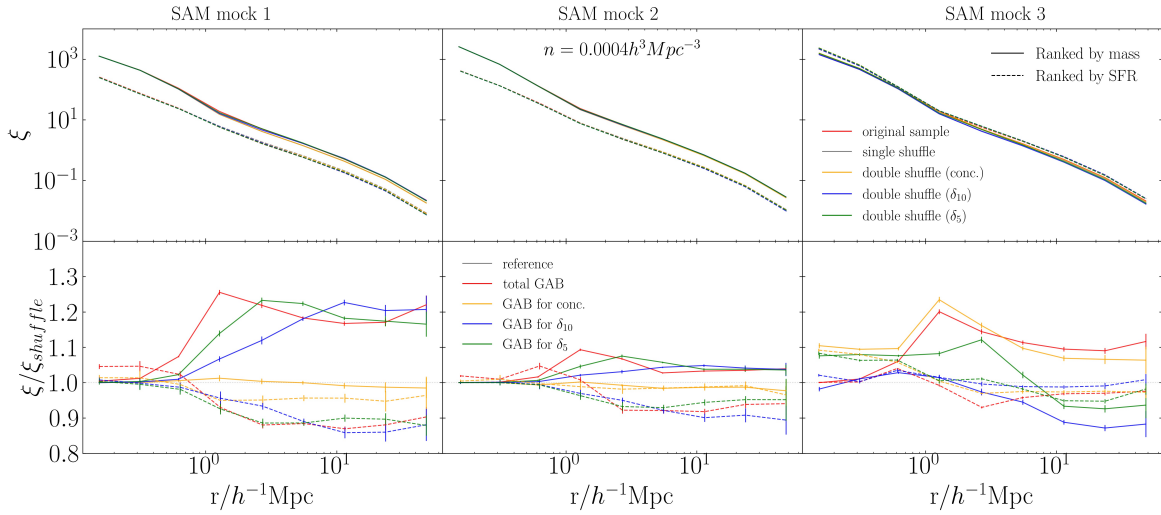


Figure 2. The GAB signals attributed to different secondary properties for three SAM mocks ($n = 0.0004h^3\text{Mpc}^{-3}$). Top panel: two-point correlation functions. The colored lines represent the original sample and various shuffled samples. Bottom panel: the ratio of correlation functions. The dashed and solid lines correspond to stellar mass- and SFR-ranked samples, respectively. The gray line represents the ratio of the correlation function with the single shuffle sample as the numerator, and its value is always 1 as a reference. The red line corresponds to the original sample, which retains total GAB signal. The yellow, blue, and green lines correspond to GAB associated with the halo concentration, environmental density δ_{10} and δ_5 . The error bars in the figure are derived from the standard deviation obtained by performing 10 random shuffle operations on the same galaxy sample, reflecting the statistical uncertainty introduced by the shuffling procedure.

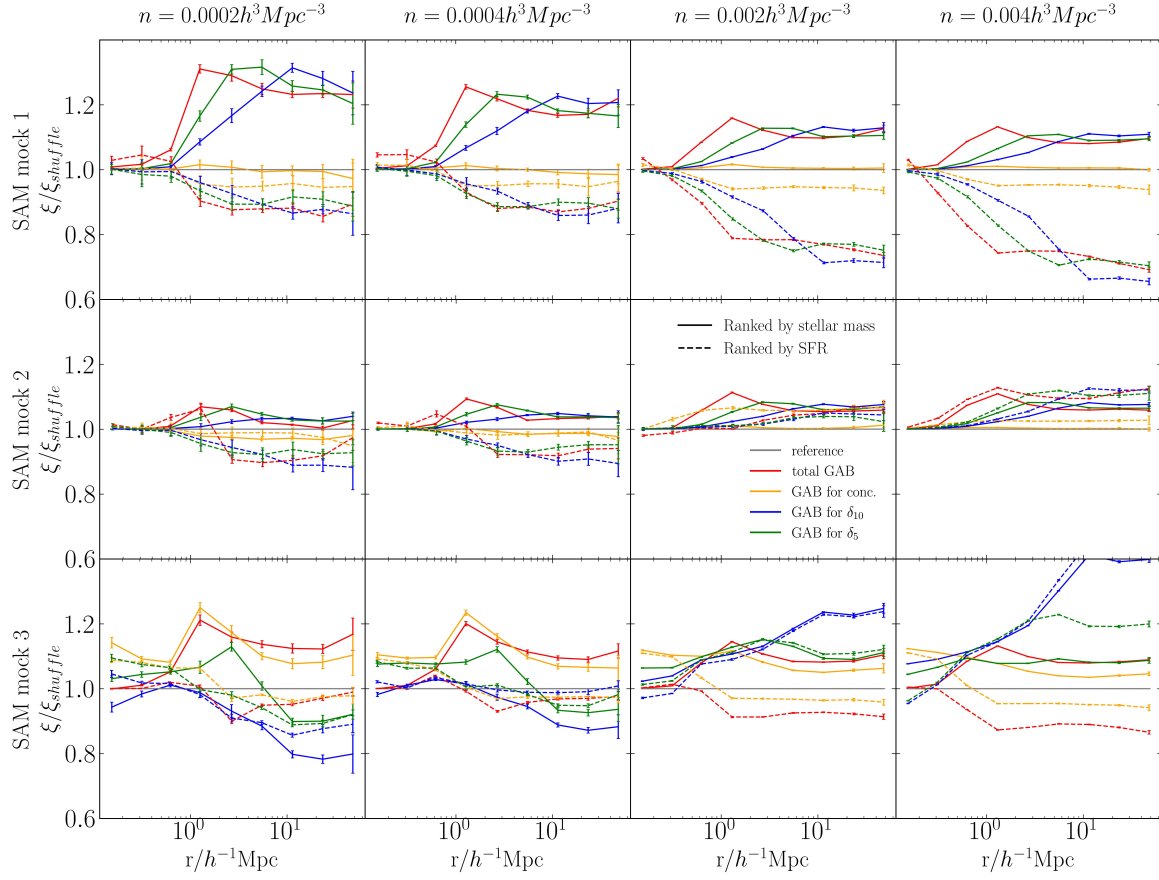


Figure 3. The same as the bottom panels of Fig. 2, but corresponding to $n = 0.004h^3\text{Mpc}^{-3}$, $n = 0.002h^3\text{Mpc}^{-3}$, $n = 0.0004h^3\text{Mpc}^{-3}$ and $n = 0.0002h^3\text{Mpc}^{-3}$.

shuffled samples. Similarly, double-shuffled samples are used to isolate the GAB contribution from a specific secondary property (concentration or local environment in this analysis). After the shuffling procedure, the HOD of the full sample (black lines in Fig. 1) remains unchanged, while the HODs of the subsamples ranked by concentration or local environment (red and blue lines in Fig. 1) become identical to that of the full sample (S. Contreras et al. 2019). To estimate the statistical uncertainty of the shuffling procedure, we repeat the shuffling process 10 times for each galaxy sample and compute the standard deviation of the resulting GAB signals. These uncertainties are shown as error bars in the figures.

Fig. 2 shows the two-point correlation functions and the GAB signals generated by different secondary properties. For illustration purposes, we present results from three representative mocks from our SAM runs. The top panel shows the two-point correlation functions for the galaxy sample with number density $n = 0.004h^3\text{Mpc}^{-3}$. The bottom panel plots the ratio of the two-point correlation functions, $\xi/\xi_{\text{single shuffle}}$. Here, the denominator $\xi_{\text{single shuffle}}$ represents a reference result with GAB signal erased. Different curves represent different choices for the numerator ξ : the original sample (red) gives the total GAB; the single-shuffled sample itself (grey) yields a constant ratio of unity as a reference; and the double-shuffled samples (yellow, blue, green) isolate the GAB contributions from concentration, δ_{10} , and δ_5 , respectively. The dashed and solid lines correspond to the result of stellar mass- and SFR-selected samples.

On small scales dominated by one-halo terms, the difference between the original and shuffled samples is negligible as expected (D. J. Croton et al. 2007), since the relative positions of galaxies within the same halo remain unchanged after shuffling. On large scales, we first note a difference between the selection criteria. For stellar-mass-selected samples, the clustering ratio is greater than unity, while for SFR-selected samples, it is less than unity (S. Contreras et al. 2019), indicating that GAB can in some cases reduce the clustering amplitude.

Regarding the contributions from different secondary properties, we find that for most of our SAM mocks, the GAB produced by δ_{10} and δ_5 is close to the total GAB, while concentration only produces a small fraction, as exemplified by SAM mocks 1 and 2. This is consistent with earlier works such as X. Xu et al. (2021a) and B. Hadzhiyska et al. (2020). However, we also find exceptions to this behavior. For example in SAM mock 3, the concentration-induced GAB becomes comparable to the total GAB on large scales, while the environment-induced GAB is suppressed and even becomes negative. This suggests that the contributions of different sec-

ondary properties can vary depending on the baryonic physics modeled by our SAM algorithms.

Fig. 3 illustrates the GAB for galaxy samples with different number densities. Based on our examination of the full set of SAM mocks, these three models represent the main types of number density dependence observed in the parameter space, but we note that this is dependent on the prescriptions of the model and the ranges of the parameter space adopted in our Galacticus modeling.

Type I (mock 1) shows a decreasing clustering ratio with increasing number density for both stellar-mass- and SFR-selected samples, consistent with X. Xu et al. (2021a), who reported a similar trend for stellar-mass-selected galaxies. Type II (mock 2) exhibits the opposite trend: the clustering ratio increases with number density for both selection criteria, with the SFR-selected sample even crossing from below unity to above unity. This pattern is similar to the findings in S. Contreras et al. (2019). Type III (mock 3) presents a more complex behavior that differs between secondary properties: the clustering ratio for environment-induced GAB increases with number density, crossing from below unity to above unity, while for concentration-induced and total GAB, it decreases. This divergent result shows that our SAM modeling is flexible in terms of sampling the underlying dark matter halo field. In addition, we note that the uncertainty increases at lower number densities due to the reduced sample size.

3.3. Relative importance of Baryonic Physics on GAB

As the previous figures show, different SAM mocks with the same number density and selection condition can predict GAB signals with different significance. This can be attributed to the strength of the astrophysical processes of each model. In this section, we explore the impact of these baryonic prescriptions on the resultant GAB signals.

Before we explore the contribution of each component, we must first define the strength of GAB signal. Following the early work by Y. Wang et al. (2025), we pick the ratio of the correlation function with and without shuffling at $r \sim 10h^{-1}\text{Mpc}$ as a proxy of the GAB measure. Given the high-dimensional space of our SAM parameters, there are multiple ways to evaluate the contribution of each parameter or physical process. For instance, we can define a fiducial model in the parameter space and then change one parameter each time and rerun the SAM. The comparison of the resultant mock and the fiducial one can provide a direct estimate of the difference. Alternatively, our analysis is based on the early work from Z. Zhai et al. (2025) that has provided hun-

dreds of SAM mocks with a Latin-hypercube sampling in the parameter space. In order to utilize these products without rerunning the SAM algorithm, we choose a different analysis strategy in this work.

We use a Random Forest (RF) regression algorithm (L. Breiman 2001) implemented in `scikit-learn` with permutation importance to analyze the impact of various galaxy formation parameters on the GAB signal. Random Forest is an ensemble method that builds multiple decision trees and aggregates their predictions. Beyond its predictive capabilities, it provides estimates of feature importance, which can measure how much each input variable contributes to explaining the variance in the target quantity.

Feature importance can be assessed through different approaches. The impurity-based method (also known as Mean Decrease in Impurity, MDI) (G. Louppe 2015) calculates the total reduction in node impurity attributable to each feature across all trees, which is the default method in `scikit-learn`. The permutation importance method (L. Breiman 2001) evaluates the importance of a feature by randomly shuffling the values of that feature and measuring the resulting drop in model performance. Unlike impurity-based importance, permutation importance does not overestimate the importance of features with many unique values, providing a more reliable estimate of each feature’s contribution to the model’s predictions. We therefore adopt permutation importance.

In our analysis, the input features are the 16 SAM parameters governing various baryonic processes, and the target variable is the amplitude of the GAB signal measured at a characteristic scale of $\sim 10 h^{-1}$ Mpc. For each feature, we compute permutation importance with 10 random shuffles; the error bars in the resultant figures of RF analysis represent the standard deviation across these 10 repetitions, reflecting the uncertainty due to the permutation procedure. This approach allows us to rank the SAM parameters according to their impact on GAB. By comparing these importance rankings across galaxy samples selected by stellar mass and SFR, we can identify which baryonic processes play a more significant role in producing GAB than the others.

In Fig. 4, we present the results of our RF analysis. The panels are arranged from left to right in order of increasing galaxy number density, revealing the difference between stellar-mass-selected (top) and SFR-selected (bottom) galaxies. Bar colors indicate different physical processes, while bar patterns distinguish the four types of GAB signals. The error bars represent the standard deviation across 10 random permutations, reflecting the stochastic uncertainty of the permutation importance procedure. The inset pie charts summarize

the relative contribution of each group of baryonic process to the total GAB signal.

For the stellar mass-selected samples, gas cooling (orange) and stellar feedback within the disk (green) play a dominant role in determining the strength of GAB. In addition, we find that this behavior does not change significantly as we increase the number density. Given the tight correlation between stellar mass and halo mass, the sample becomes more complete at the high-mass end. Therefore higher number density means the GAB signal is more dominated by less massive halos. Our analysis seems to show that baryonic effects contribute similarly across different halo masses in terms of GAB.

On the other hand, we find that for the SFR-selected samples, the contributions of baryonic effects can change significantly as we increase the number density. At low number density, the dominant process is gas cooling (orange) followed by star formation (blue). At high number density, the gas cooling process becomes the single dominant factor and the star formation parameters are no longer affecting the GAB signal significantly.

In addition to the RF analysis, we perform supplementary checks using Spearman correlation, Pearson correlation, and SHAP analyses (S. M. Lundberg & S.-I. Lee 2017). The results are broadly consistent with the RF analysis, confirming the robustness of our findings. In addition, using correlation analysis can also provide some new information. In appendix A, we present the details of the Spearman correlation result—here we only summarize it. The Pearson and SHAP results are similar in terms of the measurement.

For stellar-mass-selected samples, consistent with the Random Forest analysis, c_{multi} exhibits the strongest positive correlation with total GAB across all number densities compared to other parameters, although the correlation strength decreases with increasing density. For SFR-selected samples, the correlation patterns also align with the Random Forest analysis, reflecting the transition from star formation dominance to gas cooling dominance as number density increases: $\nu_{\text{SF},0}$ shows a weakening correlation with total GAB and concentration-based GAB, while c_{multi} exhibits a strengthening correlation. However, for environment-dependent GAB (δ_{10} and δ_5) in SFR-selected samples, f_{core} shows a consistently strong negative correlation, with little variation across number densities. These results provide additional insights into the direction and absolute strength of the correlations between each baryonic process and the GAB signal.

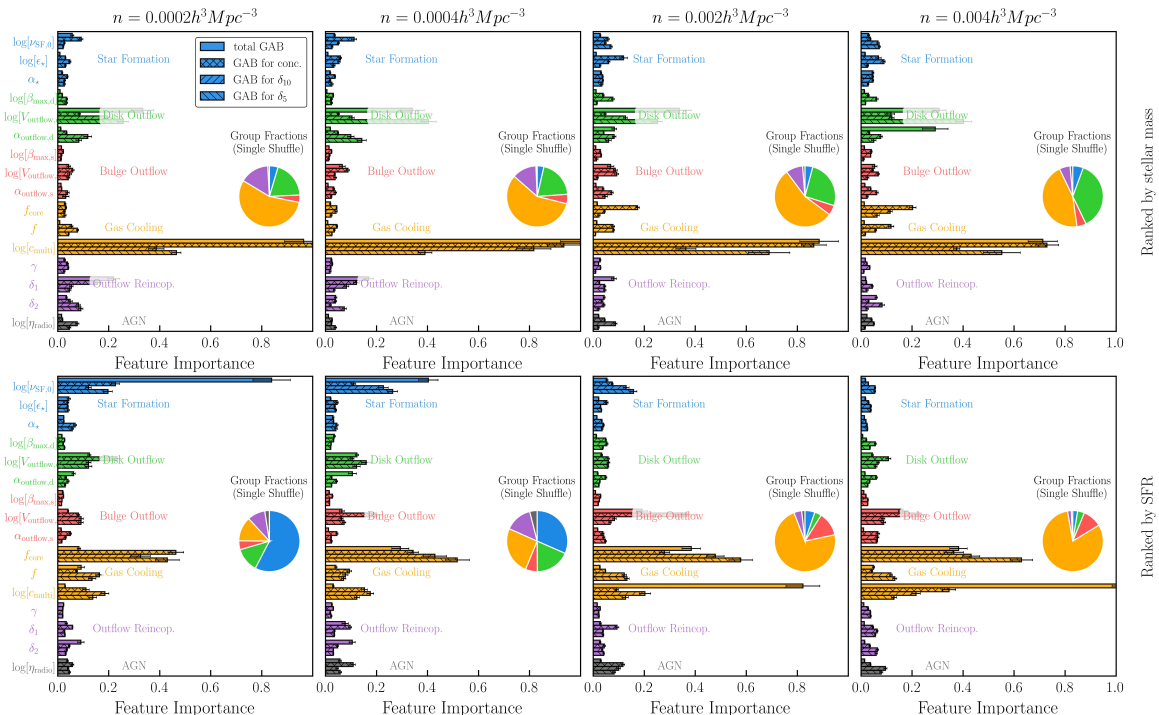


Figure 4. The relative importance of various baryonic processes on GAB. Physical processes, including star formation, stellar feedback, gas cooling, outflow reincorporation, and AGN feedback, are color-coded as shown in the legend. Bar patterns distinguish the four types of GAB signals: solid bars (total GAB), cross-hatched bars (concentration), forward-slash-hatched bars (δ_{10}), and backward-slash-hatched bars (δ_5). The error bars represent the standard deviation across 10 random permutations. The inset pie charts in each panel display the relative contribution of each physical process group to the total importance (based on the total GAB signal).

4. DISCUSSIONS AND CONCLUSIONS

In this study, we investigate the drivers of GAB, from its manifestation in OV and its dependence on secondary halo properties, to its underlying connection with the baryonic physics of galaxy formation, using the Galacticus SAM within the UNIT simulation. With hundreds of galaxy mocks that can sample the high-dimensional parameter space, we are able to explore the effect on the GAB signals in a detailed manner.

To quantify the GAB signal, we perform a traditional shuffling method, including both single shuffle and double shuffle. The *single shuffle* is performed by randomizing galaxies among halos of fixed mass, whereas the *double shuffle* further fixes a chosen secondary property, thereby isolating its specific contribution. The GAB signal is then quantified by comparing the two-point correlation functions ξ of galaxy samples before and after shuffling: we (i) use the single-shuffled sample as the GAB-free reference; (ii) the ratio $\xi_{\text{original}}/\xi_{\text{single shuffle}}$ yields the total GAB; and (iii) the ratio $\xi_{\text{double shuffle}}/\xi_{\text{single shuffle}}$ yields the GAB attributable to a particular secondary property.

We first examine the OV and GAB, isolate the contributions of concentration and local environment, and

finally uncover the correlating baryonic processes using a Random Forest machine-learning algorithm.

Our main findings are as follows:

1. While the local environment can drive stronger GAB, it does not necessarily drive stronger OV than halo concentration.
2. In most cases, environment-driven GAB is close to the total GAB, while concentration-driven GAB accounts for only a small fraction. However, we also find counterexamples (e.g., mock 3) where concentration-induced GAB exceeds environment-induced GAB. This suggests that baryonic physics can alter which secondary property drives the GAB signal.
3. The dependence of GAB on galaxy number density exhibits three distinct types across our SAM parameter space. Type I shows a decreasing clustering ratio with increasing number density for both stellar-mass- and SFR-selected samples. Type II exhibits the opposite trend, with the clustering ratio increasing with number density. Type III presents a more complex behavior: environment-induced GAB increases with number density while

concentration-induced GAB decreases. This diversity demonstrates that the impact of secondary properties on GAB is sensitive to the baryonic physics.

4. The baryonic processes responsible for GAB depend on galaxy number density and the selection criteria. For stellar-mass-selected galaxies, gas cooling and stellar feedback within the disk are consistently the dominant processes, with their relative importance largely unchanged as the number density increases. In contrast, for SFR-selected galaxies, the dominant process shifts from star formation to gas cooling as the number density increases. These rankings are robust against alternative metrics (Spearman, Pearson, SHAP), establishing a direct link between baryonic physics and the GAB.

Our study used the ratio of correlation functions to measure GAB, which was conducted in real space. A natural question is whether peculiar velocities alter this conclusion in redshift space. [N. Padilla et al. \(2019\)](#) addressed this issue by extending the shuffling technique to velocity space in a different SAM (L-GALAXIES). They found that, for both stellar-mass- and SFR-selected samples, the behaviour of the redshift-space monopole and quadrupole is qualitatively consistent with the real-space correlation function results for GAB and OV reported in [S. Contreras et al. \(2019\)](#). Moreover, the structure growth parameter f inferred from redshift-space distortions remains unbiased by GAB. This suggests that our real-space findings for the baryonic effect are likely to remain qualitatively valid in redshift space, although a dedicated redshift-space analysis with Galacticus would be needed to confirm this.

In this work, we use RF permutation importance to evaluate the contribution of individual baryonic processes to GAB. Another commonly used sensitivity analysis (SA) approach is the traditional one-at-a-time (OAT) method, which evaluates the influence of a single parameter by varying only that parameter while holding all others fixed ([M. D. Morris 1991](#)). However, the OAT method fails to capture interactions between parameters and has been noted for its limited applicability to high-dimensional, non-linear systems by [P. Oleśkiewicz & C. M. Baugh \(2019\)](#), which demonstrates that the variance-based SA method can serve as an alternative to OAT. Here, we analyse SAM mocks generated with Latin hypercube sampling using Random Forest, which naturally models complex interactions among parameters. In the process of computing permutation importance, we have effectively trained a

Random Forest regression model that learns the mapping from the 16 baryonic parameters to the GAB amplitude. A natural extension is therefore to directly use this already trained model as an emulator to rapidly predict the GAB strength for arbitrary new parameter combinations, enabling efficient exploration of the high-dimensional baryonic parameter space. The feasibility of such machine-learning-based modelling has been demonstrated, for example, by [X. Xu et al. \(2021b\)](#), who used Random Forest to predict galaxy occupation numbers from dark matter halo properties and successfully recovered the GAB signal.

In our analysis of the relative importance of baryonic physics on GAB, the scale of $10 h^{-1}\text{Mpc}$ was chosen as a proxy for the strength of GAB, following the recommendation of [Y. Wang et al. \(2025\)](#), which demonstrates that the fractional change in the clustering signal induced by assembly bias peaks at this scale. It is important to note that they focus only on assembly bias caused by the environment (δ_{10}). Our results in [Fig. 3](#) show that for the environment-induced GAB measured with δ_{10} , we indeed observe a peak in the clustering ratio at $\sim 10 h^{-1}\text{Mpc}$, consistent with [Y. Wang et al. \(2025\)](#). However, when using a smaller smoothing scale of $5 h^{-1}\text{Mpc}$ (δ_5), the peak shifts to smaller scales closer to $5 h^{-1}\text{Mpc}$. This scale-dependent behavior suggests that the characteristic scale of environmental GAB is intrinsically linked to the scale at which the environment is defined. Meanwhile, the concentration-induced GAB and total GAB exhibit peaks at even smaller scales ($\sim 1 h^{-1}\text{Mpc}$), further emphasizing that GAB for different secondary properties manifests at distinct scales. But the overall results seem to show that the choice of $\sim 10 h^{-1}\text{Mpc}$ is able to provide stable results as an evaluation of the GAB signals.

A related phenomenon that has been discussed in the context of GAB is galactic conformity. It refers to the correlation in star formation activity between central and neighboring galaxies. It was first observed within a dark matter halo (one-halo conformity; [S. M. Weinmann et al. 2006](#)) and later found to extend to scales of several Mpc (two-halo conformity; [G. Kauffmann et al. 2013](#)). [A. P. Hearin et al. \(2015\)](#) argued that this large-scale two-halo conformity is a direct manifestation of central GAB, and further proposed that it is related to large-scale tidal fields, with the signal weakening at higher redshifts ([A. P. Hearin et al. 2016a](#)). The observational results of [A. M. Berti et al. \(2017\)](#) are consistent with this prediction, supporting the interpretation that two-halo conformity reflects assembly bias. However, alternative explanations have also been proposed, suggesting that conformity may arise from mechanisms other than

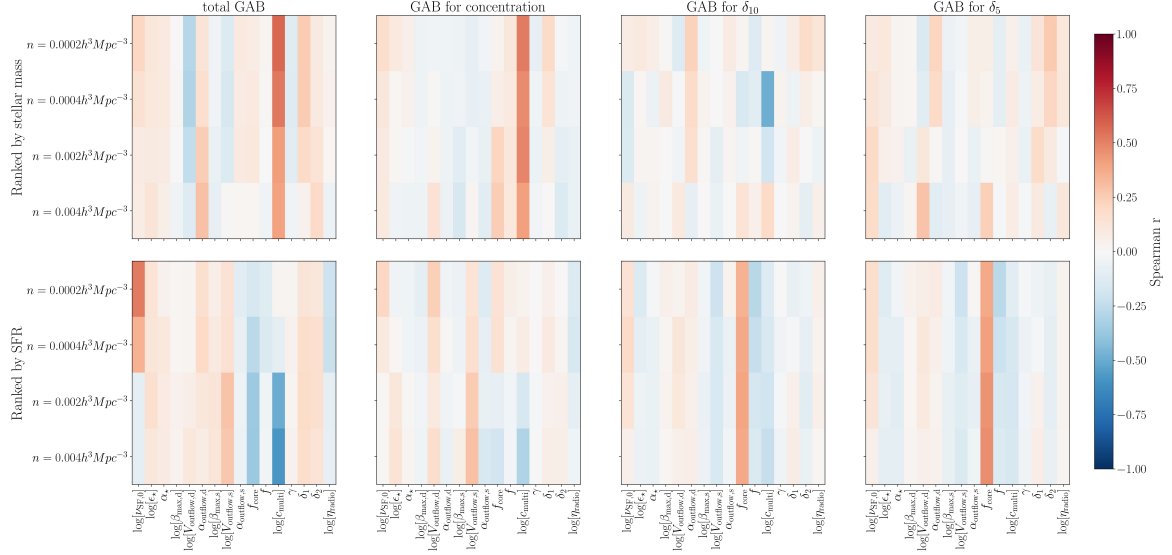


Figure 5. Spearman correlation coefficients between baryonic processes and GAB for stellar-mass-ranked (top) and SFR-ranked (bottom) samples. The y-axis shows four galaxy number densities, and the x-axis lists the SAM parameters. Red (positive) and blue (negative) colors indicate the direction and strength of correlation.

assembly bias (A. Paranjape et al. 2015; J. L. Tinker et al. 2018; Y. Zu & R. Mandelbaum 2018). On the other hand, using the semi-analytic model SAG applied to the MDPL2 simulation, Lacerna, Ivan et al. (2025) showed that the amplitudes of conformity and assembly bias are highly correlated, and both originate from environmental effects around massive dark matter halos. Our results show that GAB signals in the Galacticus SAM are significant on large scales and are primarily driven by local environmental density. A feasible test of the connection between GAB and conformity would be to compare the conformity signal before and after shuffling (especially environment-based double shuffling); we defer such investigations to a future work.

Our findings reveal that both the GAB signal and its underlying baryonic drivers differ for stellar mass- and SFR-selected galaxies. These results can provide insights for future parameterizations of GAB in empirical models, particularly regarding the distinction between luminous red galaxy (LRG) and emission-line galaxy (ELG) samples. Recently, observational studies have started to focus on GAB in ELG samples (S. Lin et al. 2022; R. Paviot et al. 2024). These results motivate extending HOD frameworks specifically for ELG samples.

Future work could incorporate not only assembly bias but also halo accretion history and baryonic process parameters informed by our Random Forest importance rankings. Such extensions will enable more accurate mock catalogs and tighter constraints on both galaxy formation physics and cosmology from next-generation surveys, including DESI (D. Collaboration et al. 2016; A. Adame et al. 2025), Euclid (R. Laureijs et al. 2011; Euclid Collaboration et al. 2022), and the Roman Space Telescope (D. Spergel et al. 2015; Y. Wang et al. 2022).

ACKNOWLEDGMENTS

ZX, JH and ZZ are supported by NSFC (12373003), the National Key R&D Program of China (2023YFA1605600), and acknowledge the generous sponsorship from Yangyang Development Fund. This work is also supported in part by the China Manned Space Program with grant no. CMS-CSST-2025-A04 and the Office of Science and Technology, Shanghai Municipal Government (grant Nos. 24DX1400100, ZJ2023-ZD-001). The computations in this paper were run on the Gravity Supercomputer at the Department of Astronomy, Shanghai Jiao Tong University.

APPENDIX

A. SPEARMAN CORRELATION ANALYSIS

Fig. 5 shows the Spearman correlation coefficients between each SAM parameter and the GAB signals. Each subplot shows the correlation strength across four galaxy number densities and 16 SAM parameters. The color bar indicates the Spearman r value, where red represents positive correlation and blue represents negative correlation. We also perform similar tests using methods including Pearson correlation and SHAP analysis, and they can yield similar results.

REFERENCES

- Abazajian, K. N., Adelman-McCarthy, J. K., Agüeros, M. A., et al. 2009, *The Astrophysical Journal Supplement Series*, 182, 543, doi: [10.1088/0067-0049/182/2/543](https://doi.org/10.1088/0067-0049/182/2/543)
- Adame, A., Aguilar, J., Ahlen, S., et al. 2025, *Journal of Cosmology and Astroparticle Physics*, 2025, 021, doi: [10.1088/1475-7516/2025/02/021](https://doi.org/10.1088/1475-7516/2025/02/021)
- Behroozi, P. S., Wechsler, R. H., & Wu, H.-Y. 2012a, *The Astrophysical Journal*, 762, 109, doi: [10.1088/0004-637X/762/2/109](https://doi.org/10.1088/0004-637X/762/2/109)
- Behroozi, P. S., Wechsler, R. H., Wu, H.-Y., et al. 2012b, *The Astrophysical Journal*, 763, 18, doi: [10.1088/0004-637X/763/1/18](https://doi.org/10.1088/0004-637X/763/1/18)
- Benson, A. J. 2010, *Physics Reports*, 495, 33, doi: <https://doi.org/10.1016/j.physrep.2010.06.001>
- Benson, A. J. 2012, *New Astronomy*, 17, 175, doi: <https://doi.org/10.1016/j.newast.2011.07.004>
- Benson, A. J., Cole, S., Frenk, C. S., Baugh, C. M., & Lacey, C. G. 2000, *Monthly Notices of the Royal Astronomical Society*, 311, 793, doi: [10.1046/j.1365-8711.2000.03101.x](https://doi.org/10.1046/j.1365-8711.2000.03101.x)
- Berlind, A. A., & Weinberg, D. H. 2002, *The Astrophysical Journal*, 575, 587, doi: [10.1086/341469](https://doi.org/10.1086/341469)
- Berti, A. M., Coil, A. L., Behroozi, P. S., et al. 2017, *The Astrophysical Journal*, 834, 87, doi: [10.3847/1538-4357/834/1/87](https://doi.org/10.3847/1538-4357/834/1/87)
- Blanton, M. R., & Berlind, A. A. 2007, *The Astrophysical Journal*, 664, 791, doi: [10.1086/512478](https://doi.org/10.1086/512478)
- Bond, J. R., Cole, S., Efsthathiou, G., & Kaiser, N. 1991, *ApJ*, 379, 440, doi: [10.1086/170520](https://doi.org/10.1086/170520)
- Breiman, L. 2001, 45, 5, doi: [10.1023/A:1010933404324](https://doi.org/10.1023/A:1010933404324)
- Chaves-Montero, J., Angulo, R. E., Schaye, J., et al. 2016, *Monthly Notices of the Royal Astronomical Society*, 460, 3100, doi: [10.1093/mnras/stw1225](https://doi.org/10.1093/mnras/stw1225)
- Chuang, C.-H., Yepes, G., Kitaura, F.-S., et al. 2019, *Monthly Notices of the Royal Astronomical Society*, 487, 48, doi: [10.1093/mnras/stz1233](https://doi.org/10.1093/mnras/stz1233)
- Cole, S., Lacey, C. G., Baugh, C. M., & Frenk, C. S. 2000, *Monthly Notices of the Royal Astronomical Society*, 319, 168, doi: [10.1046/j.1365-8711.2000.03879.x](https://doi.org/10.1046/j.1365-8711.2000.03879.x)
- Cole, S., Percival, W. J., Peacock, J. A., et al. 2005, *Monthly Notices of the Royal Astronomical Society*, 362, 505, doi: [10.1111/j.1365-2966.2005.09318.x](https://doi.org/10.1111/j.1365-2966.2005.09318.x)
- Collaboration, D., Aghamousa, A., Aguilar, J., et al. 2016, *The DESI Experiment Part I: Science, Targeting, and Survey Design*, <https://arxiv.org/abs/1611.00036>
- Colless, M., Dalton, G., Maddox, S., et al. 2001, *Monthly Notices of the Royal Astronomical Society*, 328, 1039, doi: [10.1046/j.1365-8711.2001.04902.x](https://doi.org/10.1046/j.1365-8711.2001.04902.x)
- Contreras, S., Angulo, R. E., & Zennaro, M. 2021, *Monthly Notices of the Royal Astronomical Society*, 504, 5205, doi: [10.1093/mnras/stab1170](https://doi.org/10.1093/mnras/stab1170)
- Contreras, S., Zehavi, I., Padilla, N., et al. 2019, *Monthly Notices of the Royal Astronomical Society*, 484, 1133, doi: [10.1093/mnras/stz018](https://doi.org/10.1093/mnras/stz018)
- Cooper, M. C., Gallazzi, A., Newman, J. A., & Yan, R. 2010, *Monthly Notices of the Royal Astronomical Society*, 402, 1942, doi: [10.1111/j.1365-2966.2009.16020.x](https://doi.org/10.1111/j.1365-2966.2009.16020.x)
- Cooray, A., & Sheth, R. 2002, *Physics Reports*, 372, 1, doi: [https://doi.org/10.1016/S0370-1573\(02\)00276-4](https://doi.org/10.1016/S0370-1573(02)00276-4)
- Croton, D. J., Gao, L., & White, S. D. M. 2007, *Monthly Notices of the Royal Astronomical Society*, 374, 1303, doi: [10.1111/j.1365-2966.2006.11230.x](https://doi.org/10.1111/j.1365-2966.2006.11230.x)
- Dawson, K. S., Schlegel, D. J., Ahn, C. P., et al. 2012, *The Astronomical Journal*, 145, 10, doi: [10.1088/0004-6256/145/1/10](https://doi.org/10.1088/0004-6256/145/1/10)
- Dawson, K. S., Kneib, J.-P., Percival, W. J., et al. 2016, *The Astronomical Journal*, 151, 44, doi: [10.3847/0004-6256/151/2/44](https://doi.org/10.3847/0004-6256/151/2/44)
- Drinkwater, M. J., Jurek, R. J., Blake, C., et al. 2010, *Monthly Notices of the Royal Astronomical Society*, 401, 1429, doi: [10.1111/j.1365-2966.2009.15754.x](https://doi.org/10.1111/j.1365-2966.2009.15754.x)
- Euclid Collaboration, Scaramella, R., Amiaux, J., et al. 2022, *A&A*, 662, A112, doi: [10.1051/0004-6361/202141938](https://doi.org/10.1051/0004-6361/202141938)
- Gao, L., Springel, V., & White, S. D. M. 2005, *Monthly Notices of the Royal Astronomical Society: Letters*, 363, L66, doi: [10.1111/j.1745-3933.2005.00084.x](https://doi.org/10.1111/j.1745-3933.2005.00084.x)
- Gao, L., & White, S. D. M. 2007, *Monthly Notices of the Royal Astronomical Society: Letters*, 377, L5, doi: [10.1111/j.1745-3933.2007.00292.x](https://doi.org/10.1111/j.1745-3933.2007.00292.x)

- Guo, Q., White, S., Angulo, R. E., et al. 2012, *Monthly Notices of the Royal Astronomical Society*, 428, 1351, doi: [10.1093/mnras/sts115](https://doi.org/10.1093/mnras/sts115)
- Hadzihska, B., Bose, S., Eisenstein, D., Hernquist, L., & Spergel, D. N. 2020, *Monthly Notices of the Royal Astronomical Society*, 493, 5506, doi: [10.1093/mnras/staa623](https://doi.org/10.1093/mnras/staa623)
- Hearin, A. P., Behroozi, P. S., & van den Bosch, F. C. 2016a, *Monthly Notices of the Royal Astronomical Society*, 461, 2135, doi: [10.1093/mnras/stw1462](https://doi.org/10.1093/mnras/stw1462)
- Hearin, A. P., Watson, D. F., & Bosch, F. C. v. d. 2015, *Monthly Notices of the Royal Astronomical Society*, 452, 1958, doi: [10.1093/mnras/stv1358](https://doi.org/10.1093/mnras/stv1358)
- Hearin, A. P., Zentner, A. R., van den Bosch, F. C., Campbell, D., & Tollerud, E. 2016b, *Monthly Notices of the Royal Astronomical Society*, 460, 2552, doi: [10.1093/mnras/stw840](https://doi.org/10.1093/mnras/stw840)
- Jing, Y. P., Mo, H. J., & Börner, G. 1998, *The Astrophysical Journal*, 494, 1, doi: [10.1086/305209](https://doi.org/10.1086/305209)
- Kauffmann, G., Li, C., Zhang, W., & Weinmann, S. 2013, *Monthly Notices of the Royal Astronomical Society*, 430, 1447, doi: [10.1093/mnras/stt007](https://doi.org/10.1093/mnras/stt007)
- Kravtsov, A. V., Berlind, A. A., Wechsler, R. H., et al. 2004, *The Astrophysical Journal*, 609, 35, doi: [10.1086/420959](https://doi.org/10.1086/420959)
- Lacerna, Ivan, Padilla, Nelson, & Palma, Daniela. 2025, *A&A*, 703, A247, doi: [10.1051/0004-6361/202555329](https://doi.org/10.1051/0004-6361/202555329)
- Laureijs, R., Amiaux, J., Arduini, S., et al. 2011, *Euclid Definition Study Report*, <https://arxiv.org/abs/1110.3193>
- Lehmann, B. V., Mao, Y.-Y., Becker, M. R., Skillman, S. W., & Wechsler, R. H. 2016, *The Astrophysical Journal*, 834, 37, doi: [10.3847/1538-4357/834/1/37](https://doi.org/10.3847/1538-4357/834/1/37)
- Li, Y., Mo, H. J., & Gao, L. 2008, *Monthly Notices of the Royal Astronomical Society*, 389, 1419, doi: [10.1111/j.1365-2966.2008.13667.x](https://doi.org/10.1111/j.1365-2966.2008.13667.x)
- Lin, S., Tinker, J. L., Blanton, M. R., et al. 2022, *Monthly Notices of the Royal Astronomical Society*, 519, 4253, doi: [10.1093/mnras/stac2793](https://doi.org/10.1093/mnras/stac2793)
- Lin, Y.-T., Mandelbaum, R., Huang, Y.-H., et al. 2016, *The Astrophysical Journal*, 819, 119, doi: [10.3847/0004-637X/819/2/119](https://doi.org/10.3847/0004-637X/819/2/119)
- Louppe, G. 2015, <https://arxiv.org/abs/1407.7502>
- Lundberg, S. M., & Lee, S.-I. 2017, in *31st Conference on Neural Information Processing Systems (NIPS 2017)*, Long Beach, CA, USA (Curran Associates, Inc.). <http://papers.nips.cc/paper/7062-a-unified-approach-to-interpreting-model-predictions.pdf>
- Mao, Y.-Y., Zentner, A. R., & Wechsler, R. H. 2017, *Monthly Notices of the Royal Astronomical Society*, 474, 5143, doi: [10.1093/mnras/stx3111](https://doi.org/10.1093/mnras/stx3111)
- McEwen, J. E., & Weinberg, D. H. 2018, *Monthly Notices of the Royal Astronomical Society*, 477, 4348, doi: [10.1093/mnras/sty882](https://doi.org/10.1093/mnras/sty882)
- Merson, A., Smith, A., Benson, A., Wang, Y., & Baugh, C. 2019, *Monthly Notices of the Royal Astronomical Society*, 486, 5737, doi: [10.1093/mnras/stz1204](https://doi.org/10.1093/mnras/stz1204)
- Miyatake, H., More, S., Takada, M., et al. 2016, *Phys. Rev. Lett.*, 116, 041301, doi: [10.1103/PhysRevLett.116.041301](https://doi.org/10.1103/PhysRevLett.116.041301)
- Morris, M. D. 1991, *Technometrics*, 33, 161, doi: [10.1080/00401706.1991.10484804](https://doi.org/10.1080/00401706.1991.10484804)
- Navarro, J. F., Frenk, C. S., & White, S. D. M. 1996, *ApJ*, 462, 563, doi: [10.1086/177173](https://doi.org/10.1086/177173)
- Obuljen, A., Percival, W. J., & Dalal, N. 2020, *Journal of Cosmology and Astroparticle Physics*, 2020, 058, doi: [10.1088/1475-7516/2020/10/058](https://doi.org/10.1088/1475-7516/2020/10/058)
- Oleskiewicz, P., & Baugh, C. M. 2019, *Monthly Notices of the Royal Astronomical Society*, 493, 1827, doi: [10.1093/mnras/stz3560](https://doi.org/10.1093/mnras/stz3560)
- Padilla, N., Contreras, S., Zehavi, I., Baugh, C. M., & Norberg, P. 2019, *Monthly Notices of the Royal Astronomical Society*, 486, 582, doi: [10.1093/mnras/stz824](https://doi.org/10.1093/mnras/stz824)
- Pakmor, R., Springel, V., Coles, J. P., et al. 2023, *Monthly Notices of the Royal Astronomical Society*, 524, 2539, doi: [10.1093/mnras/stac3620](https://doi.org/10.1093/mnras/stac3620)
- Paranjape, A., Kovač, K., Hartley, W. G., & Pahwa, I. 2015, *Monthly Notices of the Royal Astronomical Society*, 454, 3030, doi: [10.1093/mnras/stv2137](https://doi.org/10.1093/mnras/stv2137)
- Paviot, R., Rocher, A., Codis, S., et al. 2024, *Impact of assembly bias on clustering plus weak lensing cosmological analysis*, doi: <https://doi.org/10.1051/0004-6361/202449574>
- Peacock, J. A., & Smith, R. E. 2000, *Monthly Notices of the Royal Astronomical Society*, 318, 1144, doi: [10.1046/j.1365-8711.2000.03779.x](https://doi.org/10.1046/j.1365-8711.2000.03779.x)
- Pillepich, A., Springel, V., Nelson, D., et al. 2017, *Monthly Notices of the Royal Astronomical Society*, 473, 4077, doi: [10.1093/mnras/stx2656](https://doi.org/10.1093/mnras/stx2656)
- Planck Collaboration, Ade, P. A. R., Aghanim, N., et al. 2016, *A&A*, 594, A13, doi: [10.1051/0004-6361/201525830](https://doi.org/10.1051/0004-6361/201525830)
- Press, W. H., & Schechter, P. 1974, *ApJ*, 187, 425, doi: [10.1086/152650](https://doi.org/10.1086/152650)
- Salcedo, A. N., Zu, Y., Zhang, Y., et al. 2022, *Science China Physics, Mechanics & Astronomy*, 65, 109811, doi: [10.1007/s11433-022-1955-7](https://doi.org/10.1007/s11433-022-1955-7)
- Seljak, U. 2000, *Monthly Notices of the Royal Astronomical Society*, 318, 203, doi: [10.1046/j.1365-8711.2000.03715.x](https://doi.org/10.1046/j.1365-8711.2000.03715.x)

- Shao, Z., Zu, Y., Salcedo, A. N., et al. 2025, arXiv e-prints, arXiv:2510.20896, doi: [10.48550/arXiv.2510.20896](https://doi.org/10.48550/arXiv.2510.20896)
- Spergel, D., Gehrels, N., Baltay, C., et al. 2015, Wide-Field Infrared Survey Telescope-Astrophysics Focused Telescope Assets WFIRST-AFTA 2015 Report, <https://arxiv.org/abs/1503.03757>
- Tasitsiomi, A., Kravtsov, A. V., Wechsler, R. H., & Primack, J. R. 2004, *The Astrophysical Journal*, 614, 533, doi: [10.1086/423784](https://doi.org/10.1086/423784)
- Tinker, J. L., Hahn, C., Mao, Y.-Y., Wetzell, A. R., & Conroy, C. 2018, *Monthly Notices of the Royal Astronomical Society*, 477, 935, doi: [10.1093/mnras/sty666](https://doi.org/10.1093/mnras/sty666)
- Vale, A., & Ostriker, J. P. 2004, *Monthly Notices of the Royal Astronomical Society*, 353, 189, doi: [10.1111/j.1365-2966.2004.08059.x](https://doi.org/10.1111/j.1365-2966.2004.08059.x)
- van Daalen, M. P., Schaye, J., McCarthy, I. G., Booth, C. M., & Vecchia, C. D. 2014, *Monthly Notices of the Royal Astronomical Society*, 440, 2997, doi: [10.1093/mnras/stu482](https://doi.org/10.1093/mnras/stu482)
- Vogelsberger, M., Genel, S., Springel, V., et al. 2014, *Monthly Notices of the Royal Astronomical Society*, 444, 1518, doi: [10.1093/mnras/stu1536](https://doi.org/10.1093/mnras/stu1536)
- Walsh, K., & Tinker, J. 2019, *Monthly Notices of the Royal Astronomical Society*, 488, 470, doi: [10.1093/mnras/stz1351](https://doi.org/10.1093/mnras/stz1351)
- Wang, L., Weinmann, S. M., De Lucia, G., & Yang, X. 2013, *Monthly Notices of the Royal Astronomical Society*, 433, 515, doi: [10.1093/mnras/stt743](https://doi.org/10.1093/mnras/stt743)
- Wang, Y., Zhai, Z., Yang, X., & Tinker, J. L. 2025, *The Astrophysical Journal*, 994, 51, doi: [10.3847/1538-4357/ae0c10](https://doi.org/10.3847/1538-4357/ae0c10)
- Wang, Y., Zhai, Z., Alavi, A., et al. 2022, *ApJ*, 928, 1, doi: [10.3847/1538-4357/ac4973](https://doi.org/10.3847/1538-4357/ac4973)
- Wechsler, R. H., & Tinker, J. L. 2018, *Annual Review of Astronomy and Astrophysics*, 56, 435, doi: <https://doi.org/10.1146/annurev-astro-081817-051756>
- Wechsler, R. H., Zentner, A. R., Bullock, J. S., Kravtsov, A. V., & Allgood, B. 2006, *The Astrophysical Journal*, 652, 71, doi: [10.1086/507120](https://doi.org/10.1086/507120)
- Weinmann, S. M., van den Bosch, F. C., Yang, X., & Mo, H. J. 2006, *Monthly Notices of the Royal Astronomical Society*, 366, 2, doi: [10.1111/j.1365-2966.2005.09865.x](https://doi.org/10.1111/j.1365-2966.2005.09865.x)
- White, M., Hernquist, L., & Springel, V. 2001, *The Astrophysical Journal*, 550, L129, doi: [10.1086/319644](https://doi.org/10.1086/319644)
- White, M., Blanton, M., Bolton, A., et al. 2011, *The Astrophysical Journal*, 728, 126, doi: [10.1088/0004-637X/728/2/126](https://doi.org/10.1088/0004-637X/728/2/126)
- White, S. D. M., & Frenk, C. S. 1991, *ApJ*, 379, 52, doi: [10.1086/170483](https://doi.org/10.1086/170483)
- Wibking, B. D., Salcedo, A. N., Weinberg, D. H., et al. 2018, *Monthly Notices of the Royal Astronomical Society*, 484, 989, doi: [10.1093/mnras/sty2258](https://doi.org/10.1093/mnras/sty2258)
- Xu, X., Kumar, S., Zehavi, I., & Contreras, S. 2021b, *Monthly Notices of the Royal Astronomical Society*, 507, 4879, doi: [10.1093/mnras/stab2464](https://doi.org/10.1093/mnras/stab2464)
- Xu, X., Zehavi, I., & Contreras, S. 2021a, *Monthly Notices of the Royal Astronomical Society*, 502, 3242, doi: [10.1093/mnras/stab100](https://doi.org/10.1093/mnras/stab100)
- Yang, H.-G., Pellejero-Ibáñez, M., Peacock, J. A., & Davé, R. 2026, *Monthly Notices of the Royal Astronomical Society*, 547, 314, doi: [10.1093/mnras/stag314](https://doi.org/10.1093/mnras/stag314)
- York, D. G., Adelman, J., Anderson, Jr., J. E., et al. 2000, *The Astronomical Journal*, 120, 1579, doi: [10.1086/301513](https://doi.org/10.1086/301513)
- Yuan, S., Garrison, L. H., Hadzhiyska, B., Bose, S., & Eisenstein, D. J. 2021b, *Monthly Notices of the Royal Astronomical Society*, 510, 3301, doi: [10.1093/mnras/stab3355](https://doi.org/10.1093/mnras/stab3355)
- Yuan, S., Hadzhiyska, B., Bose, S., Eisenstein, D. J., & Guo, H. 2021a, *Monthly Notices of the Royal Astronomical Society*, 502, 3582, doi: [10.1093/mnras/stab235](https://doi.org/10.1093/mnras/stab235)
- Zehavi, I., Contreras, S., Padilla, N., et al. 2018, *The Astrophysical Journal*, 853, 84, doi: [10.3847/1538-4357/aaa54a](https://doi.org/10.3847/1538-4357/aaa54a)
- Zentner, A. R., Hearin, A., van den Bosch, F. C., Lange, J. U., & Villarreal, A. S. 2019, *Monthly Notices of the Royal Astronomical Society*, 485, 1196, doi: [10.1093/mnras/stz470](https://doi.org/10.1093/mnras/stz470)
- Zhai, Z., Benson, A., & Wang, Y. 2025, *Monthly Notices of the Royal Astronomical Society*, 544, 932, doi: [10.1093/mnras/staf1774](https://doi.org/10.1093/mnras/staf1774)
- Zhai, Z., Benson, A., Wang, Y., Yepes, G., & Chuang, C.-H. 2019, *Monthly Notices of the Royal Astronomical Society*, 490, 3667, doi: [10.1093/mnras/stz2844](https://doi.org/10.1093/mnras/stz2844)
- Zheng, Z., Berlind, A. A., Weinberg, D. H., et al. 2005, *The Astrophysical Journal*, 633, 791, doi: [10.1086/466510](https://doi.org/10.1086/466510)
- Zu, Y., & Mandelbaum, R. 2016, *Monthly Notices of the Royal Astronomical Society*, 457, 4360, doi: [10.1093/mnras/stw221](https://doi.org/10.1093/mnras/stw221)
- Zu, Y., & Mandelbaum, R. 2018, *Monthly Notices of the Royal Astronomical Society*, 476, 1637, doi: [10.1093/mnras/sty279](https://doi.org/10.1093/mnras/sty279)
- Zu, Y., Zheng, Z., Zhu, G., & Jing, Y. P. 2008, *The Astrophysical Journal*, 686, 41, doi: [10.1086/591071](https://doi.org/10.1086/591071)